Journal of the European Ceramic Society 23 (2003) 1115–1122

www.elsevier.com/locate/jeurceramsoc

Thermal conductivity of liquid phase sintered silicon carbide

L.S. Sigl[1]

Wacker Chemie GmbH, Ceramics Division, 87437 Kempten, Germany

Received 7 March 2002; received in revised form 3 July 2002; accepted 14 July 2002

Abstract

This study investigates the thermal diffusivity and conductivity of YAG/AlN-alloyed LPS-SiC as a function of composition and temperature using the laser-flash technique. Maxwell's model for the thermal conductivity of composites with spherical inclusions is adapted to typical features of the LPS-microstructure and its predictions are compared with experimental data. The results indicate that the thermal conductivity of LPS-SiC is controlled by (i) concentration of impurity atoms in the SiC-phase, (ii) fraction of bulk oxide phase and (iii) amorphous interphases which act as thermal resistance barriers.

Keywords: Interfacial thermal barrier; SiC; Sintering; Thermal conductivity; Thermal diffusivity; YAG

1. Introduction

Various engineering applications require materials which combine thermal shock resistance with durability against abrasion and low thermal distortion. Examples for such parts include gas seal rings in compressor pumps and wear linings for dewatering elements in paper machines.[1–3] Commercial products with such properties have been successfully launched during recent years by employing a new class of high strength SiC ceramics which contain oxide sintering additives.[2,3]

Suitable blends for the processing of silicon carbide include mixtures of alumina and rare earth (RE) oxides, usually yttria, or alumina/RE-oxide compounds, e.g. yttrium-aluminum garnet. Together with SiO_2 from the SiC surface and with optional sintering aids such as AlN,[2–4] the additives form a liquid phase (Liquid-Phase-Sintered SiC = LPS-SiC) at temperatures as low as 1750 °C.[5,6] The liquid promotes densification and allows consolidation to full density significantly below the temperatures required for solid state sintered SiC.[1] A vast body of literature describes various aspects of the processing of LPS-SiC.[2–12]

LPS-SiC composites feature a unique combination of strength, toughness and hardness, which is superior to the mechanical properties of sintered SiC. Two basic classes of LPS-SiC exist: (i) composites with equiaxed grains whose improved fracture resistance has been attributed to microcrack toughening at favourably oriented interfaces between SiC and YAG[13] and (ii) coarsened microstructures where toughening by in-situ formed SiC platelets was identfied as the key mechanism for improved fracture resistance.[5,14–16] The mechanical properties of LPS-SiC have been discussed in numerous studies in the recent literature, see e.g. Refs. 5–7, 12–16.

Surprisingly, the interest in thermal and electrical properties of LPS-SiC has arisen only recently,[17–19] despite the substantial research performed on LPS-SiC during the past decade. The principles governing transport properties of *single phase* SiC, both single- and polycrystalline, are well understood,[20,21] and the effects of SiC particles on the thermal diffusivity/conductivity of metallic and ceramic *composites* have been investigated.[22–27] Nevertheless, analysis of both electrical and thermal properties of LPS-SiC is scarce and the understanding of the governing mechanisms is incomplete.

This paper provides experimental data on the thermal diffusivity and conductivity of YAG/AlN-alloyed LPS-SiC with 3 up to 30 vol.% oxide phase as a function of temperature. Furthermore it aims at modeling thermal conductivity with respect to microstructural features such as volume fraction of bulk oxide phase. Finally it is attempted to clarify whether amorphous interphases act

E-mail address: lsigl@sinterstahl.com (L.S. Sigl).

[1] Present address: Sinterstahl GmbH, Hiebelerstraße 4, D-87629 Füssen, Germany.

0955-2219/03/$ - see front matter
PII: S0955-2219(02)00271-6

as thermal resistance barriers and to what extent their properties affect the thermal transport characteristics of LPS-SiC composites.

2. Experimental procedures

Submicron α-SiC (Wacker Chemie GmbH, Ceramics Division, Kempten, Germany) (BET 12.5 m^2/g, oxygen content 0.6 wt.%), pre-alloyed yttrium-aluminum garnet (3 Y_2O_3×5 Al_2O_3) and AlN (AlN Grade F, H.C. Starck GmbH, Goslar, Germany) were used as starting materials to prepare a range of SiC-YAG compositions. The yttrium-aluminum garnet (YAG) was prepared from commercial alumina (Alumina Grade A16, Alcoa Industrial Chemicals, Bauxite, AR, USA) and yttria (Yttria Grade fine, H.C. Starck GmbH, Goslar, Germany) powders by mixing, tempering at 1600 °C for 2 h and subsequent milling in a planetary ball mill to a specific surface of 2 m^2/g. The SiC powder was eventually blended with YAG and AlN powder (molar ratio YAG:AlN = 4:1) to yield LPS-SiC composites with 3, 5, 10, 20 and 30 vol.% of oxide phase in the as-sintered composites. The SiC-YAG-AlN powder blend was homogenized in a planetary ball mill for 60 min in water using SiC media and SiC containers to avoid contamination during processing.

After milling, the slurry was freeze-dried and screened. Bodies (60×20×20 mm^3) were eventually formed by cold-isostatic pressing at 200 MPa. They were subsequently heated up at 15 K/min in a graphite containment which was placed in a graphite tube resistance furnace and sintered at 1970 °C for 30 min under 0.1 MPa argon. At the end of the sintering cycle an Ar-pressure of 10 MPa was applied for 10 min. to reach full density. Weight loss after sintering was determined to be less than 1 wt.% in all composites. Specimens for measuring thermal diffusivity were then sliced from the bars and ground to form thin disks, 10 mm in diameter and 2.34 mm thick. Both faces of the disks were polished to a 1 μm finish.

Thermal diffusivity, a, of each composition was measured in the temperature range from 25 to 1000 °C using the laser-flash technique.[28] In this procedure the front face of the disk sample is subjected to a short-duration laser pulse and the thermal history of the opposite face is assessed. In the present study, the heat pulse was supplied by a 40 J neodymium laser (wavelength 1036 nm) with a 0.5 ms pulse duration, and the specimen temperature was recorded with a Ni–Ni/Cr thermocouple. The thermal diffusivity, a, was calculated from

$$a = \omega \frac{d^2}{\tau_{1/2}} \quad (1)$$

where ω is a dimensionless constant taking the value 0.139 for the present set-up, d is the thickness of the specimen, and $\tau_{1/2}$ is the time period required for the rear face of the specimen to reach half of the maximum value of temperature. Heat losses were minimized by performing the measurements in vacuum using thin alumina tubes for holding the specimen and radiation shields to reduce radiation losses. Compensation of equation (1) for finite pulse time was made by using the method of Clark and Taylor.[29] Measurements were made in steps of 100 °C during the heat-up cycle and in case of the 3 vol.% YAG specimen also during subsequent cooling. No significant deviation between heating and cooling cycle was detected. Each data point represents the mean of three individual measurements, the variation being typically less than ±2%.

The density, ρ, was determined at room temperature by the water immersion method. The room temperature density of the composites, ρ(RT), was extrapolated to high temperatures by using $\rho(T) = \rho(\mathrm{RT})/[1 + 3\alpha(T - \mathrm{RT})]$, where RT denotes room temperature, using a thermal expansion coefficient of $\alpha \approx 4.2\ 10^{-6}/K$.[1]

The specific heat, c_p, of each composite was measured in the same temperature range, using differential scanning calorimetry, with single-crystal alumina as a reference material. The experimentally obtained values for c_p compare well with c_p-data approximated by a linear rule of mixtures and specific heat values for the components SiC and YAG taken from Refs. 30, 31. The thermal conductivity, λ, was finally calculated from the relationship $\lambda = a\, c_p\, \rho$.

The microstructure of the composites was studied by scanning electron microscopy (SEM) of polished and plasma etched surfaces and by transmission electron microscopy (TEM).[a] Plasma etching of polished samples was performed with commercial plasma etching equipment. Details of ceramographic preparation, TEM-foil production and transmission electron microscopy are described elsewhere.[11] The grain size of SiC was determined as the mean intercept length, $\bar{L}$, using the linear-intercept method.[32] For comparison, the properties of a commercial SiC doped with AlN and carbon (EKasic® D, Wacker Chemie GmbH, Ceramics Division, Kempten, Germany) were also evaluated by the methods described above.

3. Results

3.1. Microstructure

Typical microstructures of LPS-SiC composites with 3 and 20 vol% of oxide phase are shown in Fig. 1a, b. Similar to the microstructures described in previous reports,[4–13] the SiC grains are predominantly equiaxed

[a] TEM investigations were kindly performed by Dr. H.J. Kleebe at the University of Bayreuth, Germany.

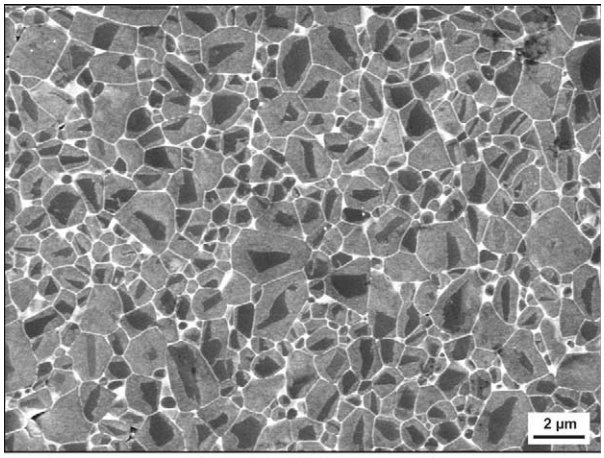

(a)

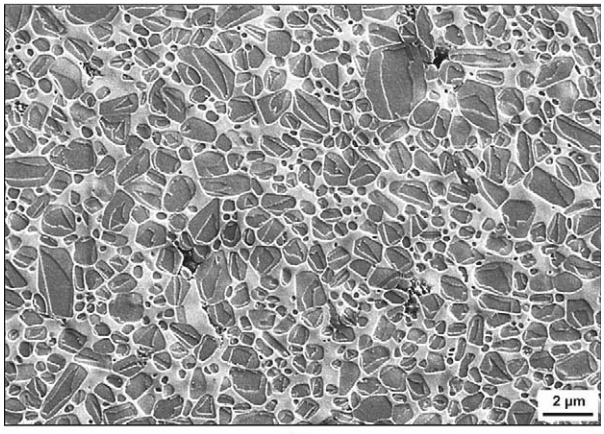

(b)

Fig. 1. SEM Micrographs of plasma-etched LPS-SiC composites with (a) 3 vol.% YAG, and (b) 20 vol% YAG. The core/rim structured SiC crystals are imbedded in a continuous YAG-matrix. SiC/SiC grain boundaries are seperated by an amorphous interphase.

with a mean grain size of $\overline{L}\approx 2$ μm and a log-normal size distribution. This microstructure is typical for soaking times <1 h and sintering temperatures below 2000 °C.[1] Specifically in the high oxide composites, it is evident that the matrix forms a continuous phase (Fig. 1b). With increasing SiC content, the SiC grains tend to agglomerate and below 20 vol.% oxide addition, the clusters constitute a three-dimensional skeleton (Fig. 1a). Thus on first sight it appears, that at low oxide contents the composites consist of two inter-penetrating, continuous networks.

SEM micrographs of plasma etched composites indicate, however, that the interfaces between SiC grains are *not* strictly contiguous, i.e. the SiC grains are covered by an interphase (Fig. 1a). This observation confirms previous TEM studies[11,13,33] and is supported by high resolution TEM micrographs, which reveal a thin layer of an amorphous phase with a typical width of ≈1.0 nm residing between SiC/SiC boundaries (Fig. 2). It is important to note, that microcracks at SiC/YAG or SiC/SiC boundaries, which might affect the thermal

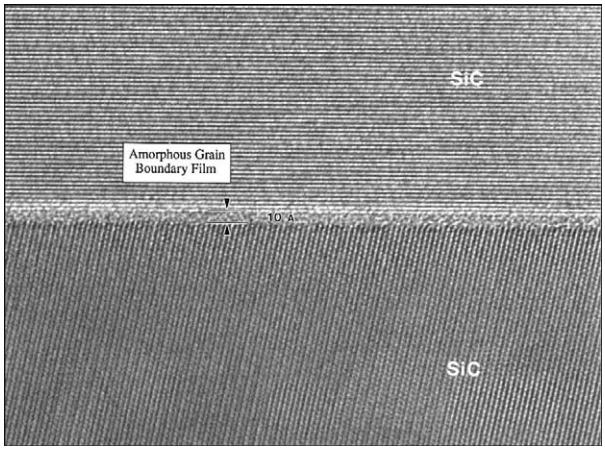

Fig. 2. TEM micrograph of a SiC/SiC grain boundary in a 5 vol.% YAG LPS-SiC composite revealing an amorphous grain boundary film with a typical width of ≈1.0 nm.

transport properties, are virtually absent in the bulk material. According to Kleebe,[13] microcracks in LPS-SiC emanate only in the stress field of a travelling crack.

X-ray inspection shows, that the oxide matrix in LPS-SiC is predominantely crystalline YAG ($Y_3Al_5O_{12}$), confirming results of previous X-ray investigations[34] and selected area diffraction experiments.[13,33] High resolution transmission micrographs reveal that besides the major phase of crystalline YAG, thin layers of amorphous oxide with a typical width of ≈1.2 nm exist at YAG/SiC interfaces (Fig. 3). Though the statistical significance of TEM observations is limited, SEM micrographs suggest that virtually all SiC grains are enveloped by amorphous oxide films (Fig. 1a), i.e. a continuous amorphous film appears to exist around SiC grains.

As reported previously, the composition of SiC crystals is heterogeneous and exhibits a core/rim structure (Fig. 1), which is due to solution and reprecipitation of SiC during sintering.[11] These investigations have revealed that the rim is slightly enriched in Al and O as compared to the initial composition of the core.[11] Thus the microstructure of LPS-SiC can be generally described as core/rim-structured SiC-crystals seperated by thin amorphous oxide layers and embedded into a fully continuous network of crystalline YAG.

3.2. Properties

The thermal diffusivity and specific heat data for all LPS-SiC composites are plotted in Figs. 4 and 5 as a function of temperature, the densities at ambient temperature are listed in Table 1. From these data the thermal conductivity was calculated from $\lambda = a c_p \rho$, and is plotted in Fig. 6 as a function of temperature. It is seen that both a and λ decline monotonously with increasing fraction of oxide phase and with increasing temperature.

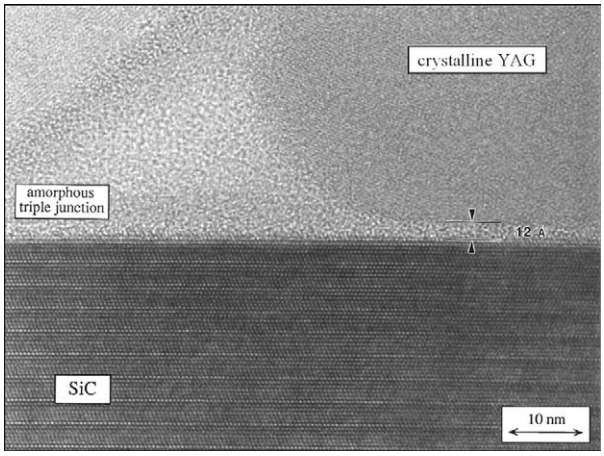

Fig. 3. TEM micrograph of a triple point area in a 5 vol.% YAG LPS-SiC composite. Note that the triple point is essentially composed of crystalline YAG. An amorphous oxide layer resides between crystalline YAG and SiC with a typical width of ≈1.2 nm.

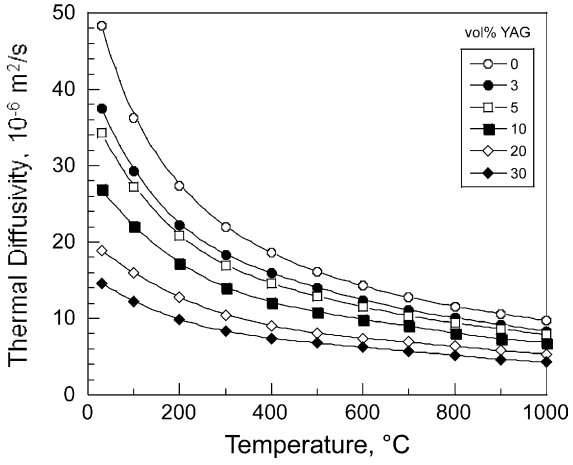

Fig. 4. Thermal diffusivity, a, of LPS-SiC YAG composites as a function of temperature. Also plotted are the data for a commercial AlN/C-doped SiC.

4. Modelling

The conductivity of a composite can be predicted provided suitable assumptions are made about the flow of heat through the constituents. Upper and lower bounds for the thermal conductivity of two-phase composites are readily derived when the constituent phases are arranged as slabs.[35] In a serial arrangement of slabs, the thermal gradient is identical in both phases, whereas in a parallel configuration the total heat flux is identical in both phases. With these restrictions and using λ_1, λ_2, f_1 and $f_2 = 1 - f_1$ to denote the thermal conductivities and volume fractions of phase 1 and phase 2 respectively, the thermal conductivity of a composite is given by[35]

$$\lambda = f_1\lambda_1 + f_2\lambda_2 \tag{2a}$$

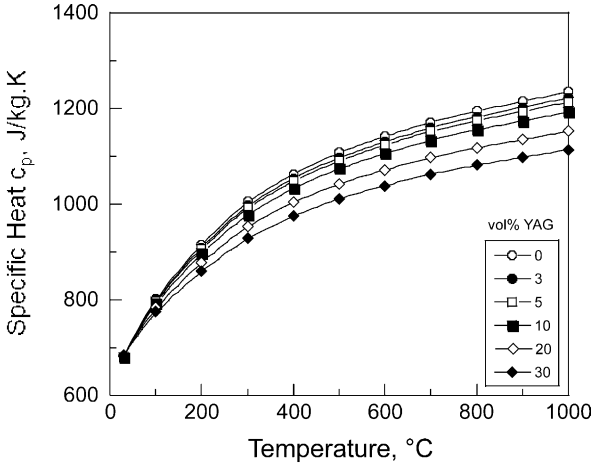

Fig. 5. Specific heat capacity, c_p, of LPS-SiC YAG composites as a function of temperature. Also plotted are the data for a commercial AlN/C-doped SiC.

Table 1
Density of LPS-SiC composites and of single-phase AlN/C-doped SiC in g/cm³ at room temperature

Volume fraction YAG, vol.%					
0 (EKasic® D)	3	5	10	20	30
3.195	3.244	3.272	3.339	3.474	3.609

The data for 100–1000 °C were calculated using $\rho(T) = \rho_{RT}/(1 + \alpha\Delta T)$ with $\alpha = 4.2\ 10^{-6}$/K.[1]

for the serial configuration. The solution for the parallel arrangement is[35]

$$\lambda = \frac{1}{f_1/\lambda_1 + f_2/\lambda_2} \tag{2b}$$

A refined model for the thermal conductivity of two-phase composites is provided by Maxwell's solution for spherical particles which are discontinuously dispersed in a continuous matrix. The thermal conductivity of the composite is given by[36,37]

$$\lambda = \lambda_m \frac{2f_p(\lambda_p/\lambda_m - 1) + \lambda_p/\lambda_m + 2}{f_p(1 - \lambda_p/\lambda_m) + \lambda_p/\lambda_m + 2} \tag{3}$$

where λ_p, λ_m, f_p and $f_m = 1 - f_p$ denote the thermal conductivities and volume fractions of the dispersed particles and the matrix respectively. It should be noted that Eq. (3) is sensitive as to whether the high- or the low-conductivity phase constitutes the matrix.

The SEM and TEM observations described above indicate, that LPS-SiC is a complex, multi-level composite material, where the following microstructural features need to be accounted for the modelling of thermal conductivity:

(i) On the first level, LPS-SiC is a composite made up of SiC-agglomerates which are dispersed in a *continuous*, crystalline YAG-matrix
(ii) The SiC agglomerates themselves are a composite material consisting of crystalline SiC surrounded by a *continuous* film of amorphous grain boundary phase
(iii) Finally, the SiC crystallites also form a composite material because they feature a core/rim structure with different amounts of elements such as Al, N, and O in solid solution.

To account for observation (i) Eq. (3) implies that the thermal conductivity of this composite is given by

$$\lambda = \lambda_{YAG}\ \frac{2(1-f_{YAG})(\lambda_A/\lambda_{YAG}-1)+\lambda_A/\lambda_{YAG}+2}{(1-f_{YAG})(1-\lambda_A/\lambda_{YAG})+\lambda_A/\lambda_{YAG}+2} \tag{4}$$

where λ_A, λ_{YAG} and f_{YAG} denote the thermal conductivities of the SiC-agglomerates and of YAG, and the volume fraction of YAG respectively. According to (ii), the thermal conductivity of the SiC-agglomerates, λ_A, with SiC particles being embedded into a continuous matrix of an amorphous grain-boundary phase is, again, expressed by Eq. (3) as

$$\lambda_A = \lambda_{GB}\ \frac{2(1-f_{GB})(\lambda_{SiC}/\lambda_{GB}-1)+\lambda_{SiC}/\lambda_{GB}+2}{(1-f_{GB})(1-\lambda_{SiC}/\lambda_{GB})+\lambda_{SiC}/\lambda_{GB}+2} \tag{5}$$

where λ_{GB} and f_{GB} denote the thermal conductivity and volume fraction of the grain boundary phase in the SiC-agglomerates respectively. Inserting Eq. (5) into Eq. (4) eventually yields the thermal conductivity of the composites as a function of the thermal conductivities of the constituent phases.

The volume fraction of the grain boundary phase in the SiC-agglomerates, f_{GB}, is readily derived by noting that

$$f_{GB} = \frac{V_{GB}}{V_{GB}+V_{SiC}} \tag{6}$$

The grain boundary phase of volme V_{GB} has a width, t_{GB}, and surrounds SiC grains of volume V_{SiC}. With the specific surface of SiC crystallites, $S_V^{SiC} = 4/\bar{L}_{SiC}$,[32] the volume of grain boundary phase, V_{GB}, is given by

$$V_{GB} = S_V^{SiC}\, V_{SiC}\, t_{GB} = \frac{4}{\bar{L}_{SiC}}\, V_{SiC}\, t_{GB} \tag{7}$$

where $\bar{L}_{SiC}$ is the mean linear intercept length of the SiC crystals. Inserting Eq. (7) into (Eq. (6) and noting that $V_{SiC} >> V_{GB}$ yields

$$f_{GB} = 4\frac{t_{GB}}{L_{SiC}} \tag{8}$$

With $t_{GB} \approx 1$ nm (Fig. 2) and $\bar{L}_{SiC} \approx 2$ μm, one obtains $f_{GB} \approx 0.2$ vol.%.

5. Discussion

With λ-values as high as 400 W/mK at RT, single-crystal SiC ranks among the best thermal conductors, being superseded only by diamond and cubic boron nitride. The thermal conductivity of *polycrystalline* SiC is, however, significantly reduced due to increased scattering of phonons at impurity atoms which are dissolved in the SiC lattice.[20–24,38] These impurities originate from the sintering aids required for the consolidation of SiC. Generally, carbon together with boron and/or aluminum and their respective compounds are used for solid state sintering of SiC, but sintering aids such as Be or BeO have also been suggested.[1] Due to the low solubility of Be in SiC, Be-doped silicon carbide can exhibit thermal conductivites up to 250 W/mK at RT. [21] The thermal conductivity of B-doped materials is reduced to λ-values of 100–150 W/mK,[20–24] due to the fact that the SiC lattice dissolves more B than Be. Al being even more soluble in SiC, further reduces the thermal conductivity of Al-doped SiC to λ-values in the range of 80–120 W/mK[1,20–24] With a thermal conductivity of 105 W/mK at RT, the λ-values of the AlN/C-doped reference material agree well with literature data.

5.1. Compositional dependence

Using Eqs. (4)–(6) to relate the microstructural features and the thermal conductivities of the individual constituents to the thermal conductivity of the composites, it will be attempted in this section to clarify the role of microstructure on the thermal transport in LPS-SiC materials. As evidenced by Fig. 6, addition of an oxide phase significantly reduces the thermal conductivity of LPS-SiC as compared to polycrystalline "single-phase" SiC. An initial check for the applicability of the models from Section 4 is made by using room temperature data only. Taking $\lambda_{RT} = 105$ W/mK for SiC with Al and N in solid solution (Fig. 6) and $\lambda_{RT} = 9.8$ W/mK for YAG[40] as thermal conductivities of the constituents at room temperature, estimates for the upper and lower bounds of the thermal conductivity of the composites are readily inferred from Eqs. (2a, b). These bounds are plotted in Fig. 7 together with experimental λ-values for the LPS-SiC ceramics (dotted lines). As expected, the experimental data for all compositions are located well within Hashin's parallel/serial boundaries.

Also plotted is the prediction of Maxwell's model [Eq. (3)] of spherical SiC-particles, dispersed in a matrix of YAG, and assuming that *no* amorphous phase is present at the SiC grain boundaries, i.e. $f_{GB}=0$. From Fig. 7 it becomes evident, that a model neglecting the grain boundary phase overestimates the thermal conductivity of LPS-SiC composites by ≈20%. It is therefore concluded that the amorphous grain boundary phase significantly reduces the thermal conductivity of LPS-SiC materials.

The effect of the grain boundary film is modelled by calculating the thermal conductivity of the SiC/grain boundary "composite" according to Eq. (5). Following Kingery[38] and Scholze,[39] the thermal conductivity of SiO_2-rich glasses is in the range 1 W/mK $<\lambda_{Glass}<3$ W/mK and stays fairly constant with increasing temperature. Combing Eqs. (4) and (5), setting λ_{SiC}, λ_{YAG}, λ_{GB} as 105, 9.8 and 2 W/mK and, as elucidated above, $f_{GB}=0.2$ vol.%, yields the fit depicted in Fig. 7 (solid line). This prediction describes the trend of the experimental data at room temperature reasonably well.

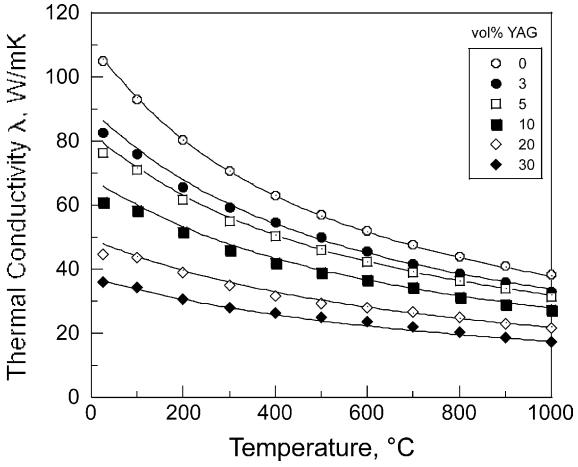

Fig. 6. Thermal conductivity, λ, of LPS-SiC YAG composites as a function of temperature. Also plotted are the data for a commercial AlN/C-doped SiC.

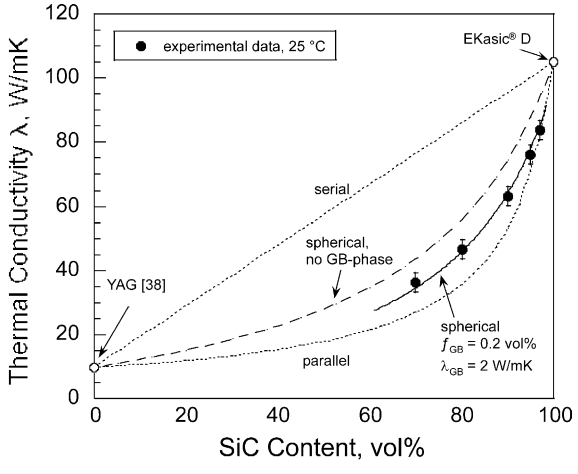

Fig. 7. Thermal conductivity, λ, of LPS-SiC YAG composites at room temperature, plotted as a function of composition (solid circles). The dashed lines represent Hashin's bounds. The dash-dotted line is a best fit according to Eqs. (4)–(6) with *no* GB-phase ($f_{GB}=0$) and with λ_{SiC}, λ_{YAG} of 105 and 9.8 W/mK respectively. The solid line is a best fit-line as above, but *with* a GB-phase setting $\lambda_{GB}=2$ W/mK and $f_{GB}=0.2$ vol.%.

5.2. Temperature dependence

Having obtained preliminary confidence in its validity, the model is further checked by fitting Eqs. (4) and (5) to the experimental λ-values of LPS-SiC composites at various temperatures, but now considering $\lambda_{SiC}(T)$ and $\lambda_{YAG}(T)$ as fit-parameters[3] with the assumption of $\lambda_{GB}(T)=$const.$=2$ W/mK and $f_{GB}=0.2$ vol.%. This procedure is intended to figure out whether increased contents of Al and O in the rim of SiC crystallites would affect the thermal conductivity of the composites. In case of a reduced thermal conductivity, the fit data for $\lambda_{SiC}(T)$ would be expected to be smaller than the experimental λ-values of the commercial AlN/C-doped SiC.

The results for the best-fit parameters are plotted in Fig. 8 and compared to the experimental $\lambda(T)$-values for the AlN/C-doped SiC and for YAG from Ref. 40. It should be noted that the results are fairly insensitive to a variation of λ_{GB} and f_{GB} within $0.5\leqslant\lambda_{GB}<3$ W/mK and $0.1\leqslant f_{GB}<0.3$ vol.%.

As can be inferred from Fig. 8, the fitted $\lambda(T)$-values of the LPS-SiC composites match very well with experimental data for AlN/C-doped SiC. From this evidence it is suggested that the core rim/structure does not significantly impact thermal conductivity of the SiC crystallites. Most likely, this behavior is due to a limited

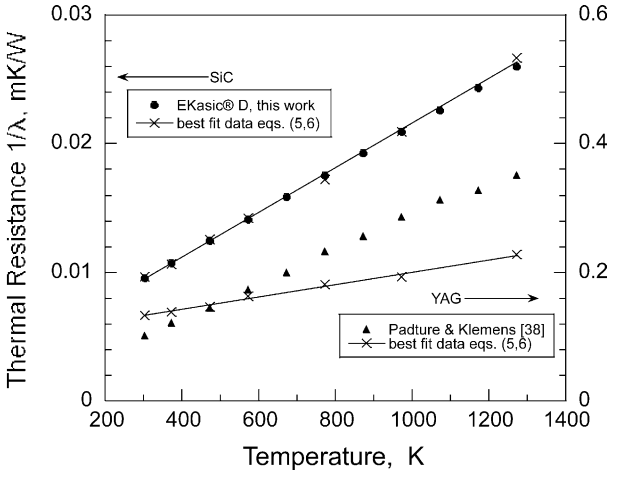

Fig. 8. Temperature dependence of "best fit" thermal resistance data of SiC and YAG compared to literature data.

[3] The data were fitted with KaleidaGraph® of Synergy Software, Reading, PA.

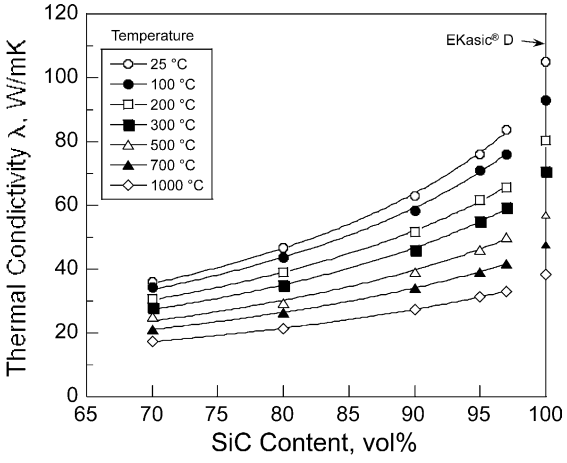

Fig. 9. Comparison of thermal conductivity of LPS-SiC composites calculated from Eqs. (4), (5) and (8) using $\lambda_{GB}=2$ W/mK and $f_{GB}=0.2$ vol.% (lines) with experimental data (symbols).

sensitivity of scattering in SiC crystals being already highly saturated with Al, N and O.

The fitted $\lambda_{YAG}(T)$-values are of the same magnitude as YAG conductivities published by Padture and Klemens [40], yet the agreement is worse than for SiC. It is hypothesized that this behavior might be due to the fact that Padture and Klemens conducted their measurements on pure YAG. The present data are inferred from YAG which due to liquid phase sintering will contain remnants of Si and C in solid solution.

Above the Debye-temperature, the temperature dependence of the thermal resistance, $1/\lambda$, of crystalline solids with phonon dominated conduction can be reasonably approximated by a linear function of the type $1/\lambda=(a+bT)$.[20,37] The best-fit-data for $\lambda_{SiC}(T)$ and $\lambda_{YAG}(T)$ from Fig. 8, both have a linear temperature dependence with the following best-fit equations

$$\frac{1}{\lambda_{SiC}(T)} = 3.81\ \ 10^{-3} + 1.73\ \ 10^{-5}\ \ T \tag{8a}$$

$$\frac{1}{\lambda_{YAG}(T)} = 1.04\ \ 10^{-1} + 9.57\ \ 10^{-5}\ \ T \tag{8b}$$

Combining these expressions with Eqs. (4) and (5) allows the temperature dependence of the thermal conductivity of LPS-SiC composites to be calculated and checked against experimental data for self consistency. The thermal conductivity of LPS-SiC composites predicted from Eqs. (4), (5) and (8) using $\lambda_{GB}(T)=2$ W/mK and $f_{GB}=0.2$ vol.%, is plotted as solid lines together with experimental λ-values in Fig. 9. It is seen that the experimental data are in reasonable agreement. It is also interesting to note, that the thermal resistance, $1/\lambda$, of the composites scales with temperature, though such behaviour of a composite material would not be necessarily expected.

6. Concluding remarks

The following conclusions can be drawn from this study:

1. The thermal conductivity of LPS-SiC is strongly affected by the oxide and nitride sintering additives which form a continous matrix. The matrix is predominantly composed of crystalline YAG and features thin amorphous layers which envelop the SiC crystallites.
2. The low conductivity of crystalline YAG reduces the overall conductivity according to a rule of mixtures which is reasonably well described by Maxwell's formula for spherical particles in a continuous matrix.
3. The amorphous grain boundary film further reduces the conductivity of LPS-SiC by ≈20%.
4. Given the low thermal conductivity of the oxide matrix, improvement of the thermal conductivity of LPS-SiC composites will be most efficient by enhancing the conductivity of the SiC phase. Some atomic species of conventional sintering additives (RE-oxides with Al_2O_3 and/or AlN) being highly soluble in SiC, constitutes however an upper bound for the room temperature conductivity of LPS-SiC at 80–90 W/mK. Further enhancement of the thermal conductivity of LPS-SiC will require the replacement of Al-compounds by sintering additives with low solubility in SiC. A promising route towards this goal has been recently described in Ref. 19 who used Y_2O_3-La_2O_3/Nd_2O_3 sintering additives to densify SiC.

Acknowledgements

I am especially grateful to Dr. Hans Joachim Kleebe, now with the University of Boulder, Colorado for performing the analytical work on the transmisson microscope and for the TEM micrographs. Thanks are also due to to Alexander Pesl and Georg Victor for collecting the experimental data and their valuable assistance in preparing the specimens.

References

1. Schwetz, K. A., Silicon carbide based hard materials. In *Handbook of Ceramic Materials*, ed. R. Riedel. Wiley-VCH, Weinheim, 2000, pp. 683–740.
2. Chia, K. Y., Böcker, W. D. G. and Storm, R. S., Silicon Carbide Bodies having High Toughness and Fracture Resistance and Method of Making Same. US Patent 5 298 470, 1994.
3. Schwetz, K. A., Sigl, L. S., Kempf, T. and Victor, G., Flüssigphasengesinterte SiC-Formkörper mit verbesserter Bruchzähigkeit sowie hohem elektrischem Widerstand und Verfahren zu ihrer Herstellung, European Patent 1 070 686, 1999.

4. Rixecker, G., Wiedmann, I., Biswas, K. and Aldinger, F., Flüssigphasensintern von Siliziumcarbid: das Additivsystem AlN-Y_2O_3. In *Werkstoffwoche 98, Vol. 7*, ed. J. Heinrich, G. Ziegler, W. Hermel and H. Riedel. Wiley-VCH Verlag GmbH, Weinheim, 1999, pp. 213–218.
5. Kim, Y. W., Mitomo, M., Emoto, H. and Lee, J. G., Effect of initial α-phase content on microstructure and mechanical properties of sintered silicon carbide. *J. Am. Ceram. Soc.*, 1998, **81**, 3136–3140.
6. Kim, Y. W., Kim, J. K., Rhee, S. H. and Kim, D. Y., Effect of initial particle size on microstructure of liquid phase sintered α-silicon carbide. *J. Eur. Ceram. Soc.*, 2000, **20**, 945–949.
7. Omori, M. and Takei, H., Pressureless sintering of SiC. *J. Am. Ceram. Soc.*, 1982, **65**, C92.
8. Negita, K., Effective sintering aids for silicon carbide ceramics: reactivities of silicon carbide with various additives. *J. Am. Ceram. Soc.*, 1986, **69**, C308–C310.
9. Kim, D. H. and Kim, C. H., Toughening behavior of silicon carbide with additions of yttria and alumina. *J. Am. Ceram. Soc.*, 1990, **73**, 1431–1434.
10. Mulla, M. A. and Krstic, V. D., Low-temperature pressureless sintering of β-SiC with aluminum oxide and yttrium oxide additions. *Am. Ceram. Soc. Bull.*, 1991, **70**, 439–443.
11. Sigl, L. S. and Kleebe, H. J., Core/rim structure of liquid phase sintered silicon carbide. *J. Am. Ceram. Soc.*, 1993, **76**, 773–776.
12. Chen, Z., Effects of gadolinia and alumina addition on the densification and toughening of silicon carbide. *J. Am. Ceram. Soc.*, 1996, **79**, 530–532.
13. Kleebe, H. J., SiC and Si_3N_4 materials with improved fracture resistance. *J. Eur. Ceram. Soc.*, 1992, **10**, 151–159.
14. Padture, N. P., In-situ-toughened silicon carbide. *J. Am. Ceram. Soc.*, 1994, **77**, 519–523.
15. Padture, N. P. and Lawn, B. R., Toughness properties of a silicon carbide with in-situ-induced heterogeneous grain structure. *J. Am. Ceram. Soc.*, 1994, **77**, 2518–2522.
16. Lu, S. G. and Kim, Y. W., Relationship between microstructure and fracture toughness of toughened silicon carbide ceramics. *J. Am. Ceram. Soc.*, 2001, **84**, 1347–1353.
17. Pesl, A., Elektrische Leitfähigkeit und Wärmeleitfähigkeit von flüssigphasengesintertem SiC. Diploma Thesis, University of Leoben, Austria, 1997.
18. Martin, H. P. and Adler, J., Design of electrical and thermal properties for liquid phase sintered silicon carbide. In *Proceedings of Materials Week 2001*, Munich, Oct. 2001, Werkstoff-Informationsgesellschaft mbH.
19. Zhan, G. D., Mitomo, M., Xie, R. J. and Mukherjee, A. K., Thermal and electrical properties in plasma-activation-sintered silicon carbide with rare-earth-oxide additives. *J. Am. Ceram. Soc.*, 2001, **84**, 2448–2450.
20. Burgemeister, E. A., von Muench, W. and Pettenpaul, E., Thermal conductivity and electrical properties of 6H silicon carbide. *J. Appl. Phys.*, 1979, **50**, 5790–5794.
21. Takeda, Y., Development of high-thermal-conductive SiC Ceramics. *Ceramic Bulletin*, 1988, **67**, 1961–1963.
22. Nakamura, K. and Maeda, K., Hot pressed SiC ceramics. In *Silicon Carbide Ceramics-2*, ed. S. Somiya and Y. Inomata. Elsevier Applied Science, London and New York, 1991, pp. 139–162.
23. Liu, D. M. and Lin, B. W., Thermal conductivity in hot-pressed silicon carbide. *Ceramics International*, 1996, **22**, 407–414.
24. North, B. and Gilchrist, K. W., Effect of impurity doping on a reaction-bonded silicon carbide. *Ceramic Bulletin*, 1981, **60**, 549–554.
25. Turner, S. P., Taylor, R., Gordon, R. H. and Clyne, T. W., Thermal conductivities of Ti-SiC and Ti-TiB_2 particulate composites. *J. Mat. Sci.*, 1993, **28**, 3969–3976.
26. Luo, J., Stevens, R. and Taylor, R., Thermal diffusivity/conductivity of magnesium oxide/silicon carbide composites. *J. Am. Ceram. Soc.*, 1997, **80**, 699–704.
27. McCluskey, P. J., Williams, R. K., Graves, R. S. and Tiegs, T. N., Thermal diffusivity/conductivity of alumina-silicon carbide composites. *J. Am. Ceram. Soc.*, 1990, **73**, 461–464.
28. Parker, W. J., Jenkins, R. J., Butler, C. P. and Abott, G. L., Flash method of determining thermal diffusivity, heat capacity and thermal conductivity. *J. Appl. Phys.*, 1961, **32**, 1679–1684.
29. Clark, L. M. and Taylor, R. E., Radiation loss in the flash method for thermal diffusivity. *J. Appl. Phys.*, 1975, **46**, 714–719.
30. Gmelin, Si-compounds. In *Handbook of Inorganic Chemistry*, 8th edn. (Supplement Volume B2, Silicon Carbide Part 1). Springer Verlag, Berlin, 1984.
31. Lukas, H. L., Max Planck Institute for Metals Research, Stuttgart, Germany, private communication, 1997.
32. Weibel, E. R., *Stereological Methods, Vol.2: Theoretical Foundations*. Academic Press, London, New York, Toronto, 1980.
33. Falk, L. K. L., Microstructural development during liquid phase sintering of silicon carbide ceramics. *J. Eur. Ceram. Soc.*, 1997, **17**, 983–994.
34. Ortiz, A. L., Cumbrera, F. L., Sánchez-Bajo, F., Guiberteau, H.Xu. and Padture, N. P., Quantitative phase composition analysis of liquid-phase sintered silicon carbide using the rietveld method. *J. Am. Ceram. Soc.*, 2000, **83**, 2282–2286.
35. Hashin, Z., Assessment of the self consistent scheme approximation: conductivity of particulate composites. *J. Comp. Mat.*, 1968, **2**, 284–289.
36. Hasselman, D. P. H. and Johnson, L. F., Effective thermal conductivity of composites with interfacial thermal barrier resistance. *J. Comp. Mat.*, 1987, **21**, 508–515.
37. Kingery, W. D., Thermal conductivity: xiv conductivity of multicomponent systems. *J. Am. Ceram. Soc.*, 1959, **42**, 617–627.
38. Kingery, W. D., Bowen, H. K. and Uhlmann, D. R., *Introduction to Ceramics*, 2nd edn.. Wiley, New York, 1976.
39. Scholze, H., *Glas: Natur, Struktur und Eigenschaften*, 2nd edn.. Springer Verlag, Berlin, Heidelberg, New York, 1977.
40. Padture, N. and Klemens, P. G., Low thermal conductivity in garnets. *J. Am. Ceram. Soc.*, 1997, **80**, 1018–1020.